Modeling aerosols on the mesoscale-γ: Treatment of soot aerosol and its radiative effects

N. Riemer,[1] H. Vogel, B. Vogel, and F. Fiedler

Institut für Meteorologie und Klimaforschung, Forschungszentrum Karlsruhe, Karlsruhe, Germany

Received 24 January 2003; revised 16 April 2003; accepted 30 May 2003; published 7 October 2003.

[1] Aerosol particles modify the transfer of solar radiation in the atmosphere. To quantify this impact, the composition and the size distribution of the aerosol have to be known. In this study, simulations with a comprehensive model system including meteorological processes, gas phase chemistry, and aerosol dynamics and chemistry were carried out to investigate the impact of aerosol particles on global radiation. The model system is applied to a summer situation in the southwestern part of Germany. The aerosol model represents the aerosol population by several overlapping modes. It originally accounted for the species sulfate, nitrate, ammonium, and water and now has been extended to treat soot. Since the optical properties of soot particles depend critically on their mixing state, the transfer of soot from the external into the internal mixture is parameterized. On the basis of the simulated aerosol distributions the optical properties of the aerosol were derived using Mie calculations. These results serve as input data for the radiative transfer calculations, where we considered the wavelength interval from 280 nm to 700 nm. The results of the radiative transfer calculations show that for the summer situation presented, the aerosol in the boundary layer reduces the downward flux of the solar radiation by up to 25 W m^{-1}. Sensitivity studies showed that up to 50% of this effect can be attributed to the impact of soot. *INDEX TERMS:* 0305 Atmospheric Composition and Structure: Aerosols and particles (0345, 4801); 3307 Meteorology and Atmospheric Dynamics: Boundary layer processes; 3329 Meteorology and Atmospheric Dynamics: Mesoscale meteorology; 3359 Meteorology and Atmospheric Dynamics: Radiative processes; *KEYWORDS:* modeling, aerosols, radiation

Citation: Riemer, N., H. Vogel, B. Vogel, and F. Fiedler, Modeling aerosols on the mesoscale-γ: Treatment of soot aerosol and its radiative effects, *J. Geophys. Res.*, *108*(D19), 4601, doi:10.1029/2003JD003448, 2003.

1. Introduction

[2] Numerous studies in the past have shown that aerosol particles significantly modify the transfer of solar radiation in the atmosphere and hence affect the climate either directly through light reflection and absorption or indirectly by inducing changes in the properties of clouds [*Graßl*, 1988; *Charlson et al.*, 1991; *Taylor and Penner*, 1994; *Boucher and Anderson*, 1995; *Feichter et al.*, 1997]. However, large uncertainties still exist in quantifying this impact [*Intergovernmental Panel on Climate Change* (*IPCC*), 2001]. Estimates of the aerosol direct effect on climate for the global average are typically between 0 and -1 W m^{-2} and for the indirect effect between -1 and -2 W m^{-2}. Compared to these values, the radiative forcing of the green house gases are in the range of +2.5 W m^{-2}. The globally averaged values for the aerosol effects on climate are not representative for their regional effects which can reach much higher values.

[3] *Liepert and Tegen* [2002] state a decrease of global radiation over the past three decades of 7 to 8 W m^{-2} in the US and an increase of 3 W m^{-2} in Germany. Changes in the local surface radiation budget, however, are important for various biological and photochemical processes at the surface and for the regional climate [*Busen and Hänel*, 1987; *Reuder et al.*, 1996; *Wendisch et al.*, 2001].

[4] Scattering and absorption depends on the size distribution and the composition of the aerosol [*Sloane*, 1984]. While some species such as sulfate, ammonium and nitrate scatter light, other species such as mineral dust and soot also absorb radiation [*Horvath*, 1993]. In cities of the Northern Hemisphere the combustion of fossil fuel dominates the sources. *Hamilton and Mansfield* [1991] moreover show that in many European cities over 90% of elemental carbon originates from traffic emissions. Especially diesel cars are considered to emit soot particles [*Brüggemann et al.*, 2000]. The concentration levels of soot vary between some hundreds of nanograms per cubic meter in unpolluted regions to several micrograms per cubic meter in urban areas.

[5] While freshly emitted soot is initially externally mixed, it can be transferred into an internal mixture by coagulation, condensation or photochemical processes [*Weingartner et al.*, 1997]. This ageing process affects the

[1]Now at Department of Mechanical and Aeronautical Engineering, University of California, Davis, Davis, California, USA.

0148-0227/03/2003JD003448$09.00

hygroscopic qualities and hence the growth behavior of the particles [*Kotzick and Nießner*, 1999] and therefore their optical properties. In addition the extinction efficiency of internally mixed soot is enhanced compared to externally mixed soot, which was first examined by *Ackerman and Toon* [1981] and further by *Horvath* [1993], *Fuller et al.* [1999], and *Lesins et al.* [2002]. Both mixing states coexist in the atmosphere [*Hughes et al.*, 2000; *Naoe and Okada*, 2001; *Okada and Hitzenberger*, 2001].

[6] *Stroem et al.* [1992] examine the process of mixing due to Brownian coagulation of a black carbon aerosol population issued from a localized source with an ambient distribution of soluble particles using a sectional box model which keeps track of both particle size and inclusion. *Fassi-Fihri et al.* [1997] use a sectional aerosol model to study the impact of internal/external aerosol mixing on the optical and hygroscopic properties of two-component aerosol populations. Coagulation is assumed to be the dominant process in the formation of mixed particles, condensation processes are not considered. The process of internal mixing of externally-mixed size distributions due to coagulation was also examined with an arbitrary number of size distributions by *Jacobson et al.* [1994]. *Kleeman et al.* [1997] developed a Lagrangian air quality model which represents the aerosol particle population as a source oriented external mixture. In this model the chemical composition of particles of the same size can evolve differently due to condensation processes according to the chemical properties of the initially emitted seed particle while coagulation is not considered.

[7] On the global scale, black carbon has been treated for instance by *Penner et al.* [1993], *Cooke and Wilson* [1996], and *Liousse et al.* [1996]. In these studies a fixed transformation rate for the black carbon aerosol changing from hydrophobic to hydrophilic is prescribed. *Seland and Iversen* [1999] calculate the transfer of black carbon particles from the external to the internal mixture on a global scale by a coagulation process without explicitly prescribing a turnover rate. A comprehensive treatment of aerosol particles in an Eulerian 3-D model including black carbon particles is given by *Jacobson* [2001]. This model is applied from the global to the urban scale for the region of Southern California and includes both coagulation and condensation as ageing processes of soot aerosol. The contribution of black carbon on global warming is quantified by *Jacobson* [2000, 2002] and *Chung and Seinfeld* [2002]. *Wilson et al.* [2001] use a mixed aerosol dynamical model on the global scale to simulate the aerosol population consisting of sulfate, black carbon, organic carbon and sea salt.

[8] Most of the previous model simulations were carried out either with box models and a detailed treatment of the aerosol dynamics or with global-scale models and a parameterized description of the aerosol phase. Box models, however, are not coupled to meteorology and cannot account for transport effects and the spatial variation of the sources. Because of the coarse grid the spatial variation of the aerosol load is poorly resolved in global models. *Jacobson* [1997b, 1998] devoted modeling studies concerning the effects of aerosols containing soot on solar radiation in the boundary layer to the mesoscale. The aerosols in these studies are represented with size bins. He used a hydrostatic model as a meteorological driver. Hence the lower limit of the horizontal resolution is on the order of 5×5 km^2 which was applied in these studies.

[9] We found it therefore worthwhile to carry out 3-D simulations with a coupled non-hydrostatic mesoscale-γ model which provides a highly resolved boundary layer, to investigate the impact of tropospheric aerosol particles on solar radiation. To approach this task, we performed three dimensional simulations for the southwestern part of Germany for cloud free conditions during summertime. An aerosol model was included in the model system to treat the particle phase explicitly. The aerosol model calculates both the composition and the size distribution of the aerosol particles using the modal approach. Within the framework of this study the aerosol model was extended to allow for the treatment of the additional species soot and will henceforth be referred to as "MADEsoot." We address the issue to describe the ageing process of soot particles which transfers soot from the external into the internal mixture to describe the aerosol as realistically as possible. Besides soot, the secondary inorganic species sulfate, ammonium, nitrate and water are considered.

[10] On the basis of the calculated aerosol particle distributions, the optical properties of the particles are determined using Mie calculations. Finally, radiative transfer calculations are carried out to quantify the impact of the modeled soot particles on solar radiation.

2. Model System

2.1. KAMM/DRAIS

[11] The comprehensive KAMM/DRAIS model system uses the non-hydrostatic mesoscale model KAMM [*Adrian and Fiedler*, 1991] as the meteorological driver. It is coupled with a surface vegetation model developed by *Schädler* [1989]. This model part gives the lower boundary conditions for temperature and humidity. The submodule DRAIS calculates the transport and diffusion of the reactive trace species. For the treatment of the chemical reactions the RADM2 gas phase chemistry mechanism [*Stockwell et al.*, 1990] is incorporated. The photolysis rate coefficients are determined with the radiation scheme of *Ruggaber et al.* [1994]. The anthropogenic emissions are precalculated, and the biogenic VOC emissions are calculated depending on the land use, the modeled temperatures, and modeled radiative fluxes [*McKeen et al.*, 1991; *Lamb et al.*, 1987; *Vogel et al.*, 1995]. For the parameterization of the NO emissions from the soil a modified scheme of *Yienger and Levy* [1995] is employed [*Ludwig et al.*, 2001].

[12] Dry deposition is parameterized by means of a big-leaf multiple resistance model [*Bär and Nester*, 1992]. The aerosol model MADEsoot [*Riemer*, 2002] is used to describe the aerosol dynamics and chemistry. The typical horizontal grid size for applications of KAMM/DRAIS ranges from 1 km to 5 km. In the vertical direction 25 layers are used. The vertical grid size varies from 20 m close to the surface up to 400 m at the top of the model domain at 8 km above sea level. The time steps are on the order of seconds, and the whole model system runs in a coupled mode.

[13] The land use data are available with a horizontal resolution of 30×30 m^2. Consequently, the biogenic VOC and NO emissions and the deposition fluxes are calculated

with this high resolution. The calculated emissions and deposition fluxes are then integrated over the grid size of the individual simulations using a technique described by *Vogel et al.* [1995]. Using this subgrid method, the high resolution of the land use data is utilized.

[14] As in all limited area models, boundary conditions play an important role. In this study the following procedure is used to determine the inflow boundary conditions for the chemical species. The emissions of the area sources inside the model domain are averaged along a 20 km wide strip along the inflow boundaries. An area source with a source strength of the averaged values is given at every grid point of the inflow boundary at every time step. At the inflow boundaries the complete 3-D equations are solved assuming that $\partial c_i/\partial x_j = 0$, where c_i is the concentration of species i and x_j is the coordinate perpendicular to the boundary. This means that all physical and chemical processes at the inflow boundaries are treated consistently with the rest of the model domain. Therefore our inflow boundary conditions are based on the assumption that there is a homogeneous area upwind of the model domain with typical and identical emissions at each surface grid point. In the past, KAMM/DRAIS has been extensively validated against observations

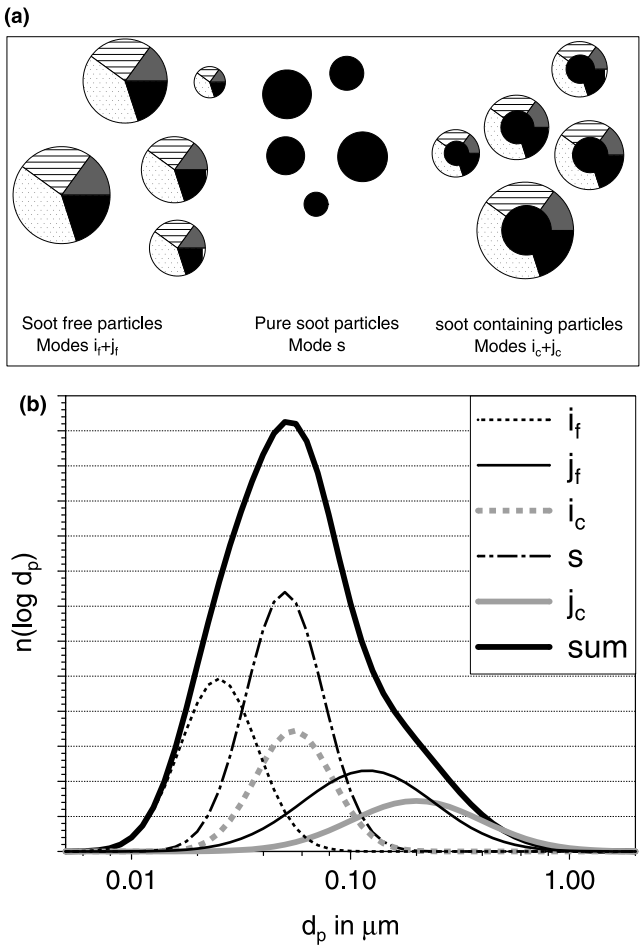

Figure 1. (a) Sketch of the individual particle classes in MADEsoot. (b) Sketch of the individual modes for the number size distribution. Summation gives the total number size distribution.

Table 1. Chemical Composition of the Individual Modes in MADEsoot

Mode l	SO_4^{2-}	NH_4^+	NO_3^-	H_2O	Soot	$\sigma_{g,l}$
$\mathbf{i_f}$	x	x	x	x		1.7
$\mathbf{j_f}$	x	x	x	x		2.0
$\mathbf{i_c}$	x	x	x	x	x	1.7
$\mathbf{j_c}$	x	x	x	x	x	2.0
s					x	1.8

[*Vogel et al.*, 1995; *Nester et al.*, 1995; *Fiedler et al.*, 2000; *Corsmeier et al.*, 2002; *Hammer*, 2001]. In the current application of the model system we will not simulate a specific episode but a typical summer situation. Therefore no comparison of observed meteorological parameters and the gas phase concentrations will be presented.

2.2. MADEsoot

[15] The aerosol model MADEsoot is used to calculate the size distribution and the chemical composition of the atmospheric particles. It is based on the Modal Aerosol Dynamics Model for Europe (MADE) [*Ackermann et al.*, 1998]. While the secondary inorganic particles treated by MADE are composed of sulfate, ammonium, nitrate and water in a completely internal mixture, we added soot in external and internal mixture as an additional component as it is depicted in Figure 1a. The aerosol population of the submicron particles is represented by several overlapping modes, which are approximated by lognormal functions. Figure 1b shows schematically the individual modes of the number density distribution, and Table 1 gives the chemical composition of the individual modes. The model generally allows also for the treatment of a coarse mode. However, the present study focuses exclusively on the impact of the fine particle fraction and the coarse mode is not considered. Freshly nucleated particles from the binary nucleation of sulfuric acid and water are assigned to mode $\mathbf{i_f}$. Modes $\mathbf{i_f}$ and $\mathbf{j_f}$ describe the soot free particles, which contain sulfate, nitrate, ammonium and water in an internal mixture. Modes $\mathbf{i_c}$ and $\mathbf{j_c}$ contain the same species as modes $\mathbf{i_f}$ and $\mathbf{j_f}$ together with soot. Mode **s** is reserved for externally mixed, pure soot.

[16] In the following, the basic concepts and equations of MADEsoot are shortly outlined. Each of the number distributions shown in Figure 1b are given by the following equation:

$$n_l(d_p) = \frac{N_l}{\sqrt{2\pi}\, d_p \,\ln \sigma_{gl}} \exp\left(-\frac{\left(\ln d_p - \ln d_{pg,l}\right)^2}{2 \ln^2 \sigma_{gl}}\right). \quad (1)$$

The subscript l indicates the individual mode ($l = \mathbf{i_f}, \mathbf{j_f}, \mathbf{i_c}, \mathbf{j_c}, \mathbf{s}$), N_l is the total number density in mode l, d_p is the diameter of the particles, σ_{gl} is the geometric standard deviation and $d_{pg,l}$ is the median diameter of mode l. The modal approach is based on the aim to predict the change of the size distribution in respect to time. The kth moment $M_{k,l}$ of the mode l is defined as:

$$M_{k,l} = \int_0^\infty d_p^k n_l(d_p)\,\mathrm{d}d_p = N_l d_{pg,l}^k \exp\left(\frac{k^2}{2} \ln^2 \sigma_{gl}\right) \quad (2)$$

[17] Generally, from the knowledge of three arbitrary moments of the distribution the three parameters $N_l = M_{0,l}$, σ_{gl} and $d_{pg,l}$ can be determined.

[18] In MADEsoot, σ_{gl} is a fixed value (numbers are given in Table 1), therefore only two moments have to be predicted. While this simplification lowers the computational effort significantly, the model comparison by *Zhang et al.* [1999] shows that problems can arise because the model cannot describe a narrowing or broadening of a mode.

[19] In the following, the zeroth moments, which are identical to the total number density and the third moments, which are proportional to the total mass density, are used to determine the median diameter $d_{pg,l}$ of the lognormal distributions. The median diameter is given by

$$d_{pg,l} = \sqrt[3]{\frac{M_{3,l}}{N_l} \exp\left(-\frac{9}{2} \ln^2 \sigma_{gl}\right)}. \quad (3)$$

For the zeroth and the third moments of each mode balance equations have to be solved. Since our aerosol particles consist at maximum of five species, the third moment $M_{3,l}$ of a mode l is the sum of the third moments of the individual species $M_{3,l,n}$:

$$M_{3,l} = \sum_{n=1}^{n_{\text{spec}}(l)} M_{3,l,n} = \sum_{n=1}^{n_{\text{spec}}(l)} \frac{m_{l,n}}{\frac{\pi}{6}\rho_n} \quad l = i_f, j_f, i_c, j_c, s \quad (4)$$

$m_{n,l}$ is the mass concentration of species n in mode l, which is proportional to the individual moment $M_{3,l,n}$ with the density ρ_n as proportionality factor. $n_{\text{spec}}(l)$ is the number of species in mode l. For the respective species in the individual modes, see Table 1.

[20] The binary nucleation of sulfuric acid and water is implemented as a source mechanism for the secondary aerosol particles. Transport, turbulent diffusion, sedimentation, deposition, coagulation and condensation are additional processes, which determine the temporal development of the individual moments and modes.

[21] The transfer of soot from the external into the internal mixture is described in the following way. Two processes can effect this transfer, coagulation and condensation.

[22] Table 2 shows how the particles, which are newly formed after coagulation, are assigned to the different modes. The interactions between all modes are considered, therefore 15 coagulation coefficients are calculated. The basic principles of the assignment to the individual modes follow *Whitby et al.* [1991]: (1) Particles formed by intramodal coagulation stay in their original modes. (2) Particles formed by intermodal coagulation are assigned to the mode with the larger median diameter.

[23] As a second process, condensation of sulfuric acid on the soot particles is included, which leads to a transfer of soot into the internal mixture as well. To retain the mode **s** for the pure soot particles, a criteria must be chosen, which determines when the aged soot together with the soluble mass of the shell is moved to the modes $\mathbf{i_c}$ and $\mathbf{j_c}$. *Weingartner et al.* [1997] show that atmospheric particles can be divided into "more hygroscopic" and "less hygroscopic" depending on their growth behavior when they are exposed to a relative humidity above 90%. On the basis of their findings we define that all material of mode **s** is moved to modes $\mathbf{i_c}$ and $\mathbf{j_c}$ if the shell mass of mode **s** rises above 5 percent. Hence the sources of the modes $\mathbf{i_c}$ and $\mathbf{j_c}$ are coagulation and condensation. Photochemical ageing [*Kotzick and Nießner*, 1999], which can also cause a transfer of soot from the external into the internal mixture is not considered in this study.

Table 2. Assignment of the Particles to the Different Modes After Coagulation

	$\mathbf{i_f}$	$\mathbf{j_f}$	$\mathbf{i_c}$	$\mathbf{j_c}$	**s**
$\mathbf{i_f}$	i_f	j_f	i_c	j_c	i_c
$\mathbf{j_f}$		j_f	j_c	j_c	j_c
$\mathbf{i_c}$			i_c	j_c	i_c
$\mathbf{j_c}$				j_c	j_c
s					s

[24] Finally, the following balance equations are solved numerically.

$$\frac{\partial}{\partial t}N_{i_f} = T(N_{i_f}) + D(N_{i_f}) - \hat{v}_{\text{sed}_{N,i_f}} \frac{\partial N_{i_f}}{\partial z} - \text{Ca}_{N,i_f i_f} - \text{Ca}_{N,i_f j_f} - \text{Ca}_{N,i_f i_c} - \text{Ca}_{N,i_f j_c} - \text{Ca}_{N,i_f s} + \text{Nu}_N \quad (5a)$$

$$\frac{\partial}{\partial t}N_{j_f} = T(N_{j_f}) + D(N_{j_f}) - \hat{v}_{\text{sed}_{N,j_f}} \frac{\partial N_{j_f}}{\partial z} - \text{Ca}_{N,j_f j_f} - \text{Ca}_{N,j_f i_c} - \text{Ca}_{N,j_f j_c} - \text{Ca}_{N,j_f s} \quad (5b)$$

$$\frac{\partial}{\partial t}N_{i_c} = T(N_{i_c}) + D(N_{i_c}) - \hat{v}_{\text{sed}_{N,i_c}} \frac{\partial N_{i_c}}{\partial z} - \text{Ca}_{N,i_c i_c} - \text{Ca}_{N,i_c j_c} - \text{Ca}_{N,i_c j_f} + \text{Ca}_{N,i_f s} \quad (5c)$$

$$\frac{\partial}{\partial t}N_{j_c} = T(N_{j_c}) + D(N_{j_c}) - \hat{v}_{\text{sed}_{N,j_c}} \frac{\partial N_{j_c}}{\partial z} - \text{Ca}_{N,j_c j_c} + \text{Ca}_{N,j_f i_c} + \text{Ca}_{N,j_f s} \quad (5d)$$

$$\frac{\partial}{\partial t}N_s = T(N_s) + D(N_s) - \hat{v}_{\text{sed}_{N,s}} \frac{\partial N_s}{\partial z} - \text{Ca}_{N,ss} - \text{Ca}_{N,i_f s} - \text{Ca}_{N,j_f s} - \text{Ca}_{N,i_c s} - \text{Ca}_{N,j_c s} \quad (5e)$$

[25] Here, the terms $T(A)$ and $D(A)$ represent the processes of advection and turbulent diffusion of the quantity A.

$$T(A) = -\bar{u}\frac{\partial A}{\partial x} - \bar{v}\frac{\partial A}{\partial y} - \bar{w}\frac{\partial A}{\partial z} \quad (6)$$

$$D(A) = \frac{\partial}{\partial x}K_{hx}\frac{\partial A}{\partial x} + \frac{\partial}{\partial y}K_{hy}\frac{\partial A}{\partial y} + \frac{\partial}{\partial z}K_{hz}\frac{\partial A}{\partial z} \quad (7)$$

[26] The variables $\bar{u}$, $\bar{v}$, $\bar{w}$ are the components of the mean wind velocity, $\hat{v}_{\text{sed}_{N,l}}$ is the sedimentation velocity for the zeroth moment of the mode l. The coefficients K_{hx}, K_{hy}, K_{hz} are the diffusion coefficients for heat with $K_{hx} = K_{hy} = 2.3\ K_{hz}$ [*Dorwarth*, 1985]. The spatial and temporal distribution of these variables are determined online by KAMM/DRAIS. The terms $\text{Ca}_{N,l_1 l_2}$ describe the change of the number density due to coagulation between particles of modes l_1 and l_2. The term Nu_N describes the increase of the number density due to nucleation.

[27] In addition to the balance equations for the number density, the balance equations for the mass concentration are solved. Since a thermodynamical equilibrium is assumed for the system of sulfate, nitrate, ammonium and water, only sulfate and soot are treated prognostically. This leads to the following equations:

$$\frac{\partial}{\partial t} m_{\mathrm{sulf},i_f} = T\left(m_{\mathrm{sulf},i_f}\right) + D\left(m_{\mathrm{sulf},i_f}\right) - \hat{v}_{\mathrm{sed}_{m,i_f}} \frac{\partial m_{\mathrm{sulf},i_f}}{\partial z} - \left(\mathrm{Ca}_{3,i_f j_f} + \mathrm{Ca}_{3,i_f j_c} + \mathrm{Ca}_{3,i_f i_c} + \mathrm{Ca}_{3,i_f s}\right) \frac{m_{\mathrm{sulf},i_f}}{M_{3,i_f}} + \mathrm{Co}_{m,i_f} + \mathrm{Nu}_m \tag{8a}$$

$$\frac{\partial}{\partial t} m_{\mathrm{sulf},j_f} = T\left(m_{\mathrm{sulf},j_f}\right) + D\left(m_{\mathrm{sulf},j_f}\right) - \hat{v}_{\mathrm{sed}_{m,j_f}} \frac{\partial m_{\mathrm{sulf},j_f}}{\partial z} - \left(\mathrm{Ca}_{3,j_f j_c} + \mathrm{Ca}_{3,j_f i_c} + \mathrm{Ca}_{3,j_f s}\right) \frac{m_{\mathrm{sulf},j_f}}{M_{3,j_f}} + \mathrm{Ca}_{3,i_f j_f} \frac{m_{\mathrm{sulf},i_f}}{M_{3,i_f}} + \mathrm{Co}_{m,j_f} \tag{8b}$$

$$\frac{\partial}{\partial t} m_{\mathrm{sulf},i_c} = T\left(m_{\mathrm{sulf},i_c}\right) + D\left(m_{\mathrm{sulf},i_c}\right) - \hat{v}_{\mathrm{sed}_{m,i_c}} \frac{\partial m_{\mathrm{sulf},i_c}}{\partial z} + \left(\mathrm{Ca}_{3,i_f i_c} + \mathrm{Ca}_{3,i_f s}\right) \frac{m_{\mathrm{sulf},i_f}}{M_{3,i_f}} - \left(\mathrm{Ca}_{3,i_c j_c} + \mathrm{Ca}_{3,i_c j_f}\right) \frac{m_{\mathrm{sulf},i_c}}{M_{3,i_c}} + \mathrm{Co}_{m,i_c} \tag{8c}$$

$$\frac{\partial}{\partial t} m_{\mathrm{sulf},j_c} = T\left(m_{\mathrm{sulf},j_c}\right) + D\left(m_{\mathrm{sulf},j_c}\right) - \hat{v}_{\mathrm{sed}_{m,j_c}} \frac{\partial m_{\mathrm{sulf},j_c}}{\partial z} + \mathrm{Ca}_{3,i_f j_c} \frac{m_{\mathrm{sulf},i_f}}{M_{3,i_f}} + \left(\mathrm{Ca}_{3,i_c j_c} + \mathrm{Ca}_{3,i_c j_f}\right) \frac{m_{\mathrm{sulf},i_c}}{M_{3,i_c}} + \left(\mathrm{Ca}_{3,j_f j_c} + \mathrm{Ca}_{3,j_f s} + \mathrm{Ca}_{3,j_f i_c}\right) \frac{m_{\mathrm{sulf},j_f}}{M_{3,j_f}} + \mathrm{Co}_{m,j_c} \tag{8d}$$

$$\frac{\partial}{\partial t} m_{s,i_c} = T\left(m_{s,i_c}\right) + D\left(m_{s,i_c}\right) - \hat{v}_{\mathrm{sed}_{m,i_c}} \frac{\partial m_{\mathrm{s},i_c}}{\partial z} + \left(\mathrm{Ca}_{3,si_f} + \mathrm{Ca}_{3,si_c}\right) \frac{m_s}{M_{3,s}} - \left(\mathrm{Ca}_{3,i_c j_c} + \mathrm{Ca}_{3,i_c j_f}\right) \frac{m_{s,i_c}}{M_{3,i_c}}$$

$$\frac{\partial}{\partial t} m_{s,j_c} = T\left(m_{s,j_c}\right) + D\left(m_{s,j_c}\right) - \hat{v}_{\mathrm{sed}_{m,j_c}} \frac{\partial m_{\mathrm{s},j_c}}{\partial z} + \left(\mathrm{Ca}_{3,sj_f} + \mathrm{Ca}_{3,sj_c}\right) \frac{m_s}{M_{3,s}} + \left(\mathrm{Ca}_{3,i_c j_c} + \mathrm{Ca}_{3,i_c j_f}\right) \frac{m_{s,i_c}}{M_{3,i_c}}$$

$$\frac{\partial}{\partial t} m_s = T(m_s) + D(m_s) - \hat{v}_{\mathrm{sed}_{m,s}} \frac{\partial m_{\mathrm{s}}}{\partial z} - \left(\mathrm{Ca}_{3,si_f} + \mathrm{Ca}_{3,si_c} + \mathrm{Ca}_{3,sj_f} + \mathrm{Ca}_{3,sj_c}\right) \frac{m_s}{M_{3,s}} \tag{8e}$$

[28] The variables $m_{\mathrm{sulf},l}$ and $m_{s,l}$ represent the mass concentrations of sulfate and soot, respectively, in the mode l. The variable m_s is the mass concentration of soot in the mode **s**. $\hat{v}_{\mathrm{sed}_{m,l}}$ is the sedimentation velocity with respect of the mass in mode l. The terms $\mathrm{Ca}_{3,l_1 l_2}$ describe the rate of transfer of third moment of mode l_1 due to the coagulation between particles of mode l_1 and l_2, $\mathrm{Co}_{m,l}$ is the condensational loss or gain of mass and Nu_m is the increase of mass due to nucleation. For a detailed description of the parameterization of the terms $\mathrm{Ca}_{N,l_1 l_2}$, $\mathrm{Ca}_{3,l_1 l_2}$ and $\mathrm{Co}_{m,l}$, see *Whitby et al.* [1991]. The treatment of the sedimentation and dry deposition, coagulation, condensation nucleation and the thermodynamical equilibrium of the aerosol species is described by *Binkowski and Shankar* [1995] and *Ackermann et al.* [1998, and references therein].

2.3. Calculations of the Optical Properties of the Aerosol Particles

[29] The optical properties of a particle population are determined by the extinction coefficient, the absorption coefficient and the phase function. The latter describes the angular distribution of the scattered radiation. These parameters are commonly needed as input data for radiative transfer calculations.

[30] The volume extinction coefficient b_e of an aerosol populations, which is represented by L overlapping modes, each with the number density distribution $n_l\left(\vec{x}, d_p\right)$ at the location $\vec{x}$ is given by

$$b_e(\vec{x}, \lambda) = \sum_{l=1}^{L} b_{e,l}(\vec{x}, m_l, \lambda), \tag{9}$$

$$b_{e,l}(\vec{x}, m_l, \lambda) = \int_{-\infty}^{\infty} \frac{\pi d_p^2}{4} Q_e\left(\vec{x}, m_l, d_p, \lambda\right) n_l\left(\vec{x}, d_p\right) \mathrm{d}d_p, \tag{10}$$

where m_l is the refraction index of the particles in mode l, Q_e the extinction efficiency, λ the wavelength of the incident radiation and d_p the diameter of the particles. The extinction efficiency Q_e is the sum of the scattering efficiency Q_s and the absorption efficiency Q_a:

$$Q_e = Q_s + Q_a. \tag{11}$$

Correspondingly, the volume extinction coefficient b_e is composed of the volume absorption coefficient b_a and the volume scattering coefficient b_s:

$$b_e = b_s + b_a. \tag{12}$$

Since we assume spherical particles, the extinction efficiency can be calculated using Mie theory. This method provides the partitioning of the extinction coefficient into the absorption and the scattering coefficient as well as the phase function. For our study we use a Mie code according to *Bohren and Huffman* [1983] for homogeneous and coated spheres. Since we treat internally mixed particles a mixing rule is needed to calculate the composite refractive index as it is described, for instance, by *Jacobson* [1997a]. In the case of solutions as it applies to the particles in the soot-free modes $\mathbf{i_f}$ and $\mathbf{j_f}$ and the shell of the soot-containing modes $\mathbf{i_c}$ and $\mathbf{j_c}$, the composite refraction index $\bar{m}$ can be computed as a volume-weighted average of the n_{spec} individual refractive indices m_n [*Hänel*, 1976]

$$\bar{m} = \sum_{n=1}^{n_{\mathrm{spec}}} f_n m_n, \tag{13}$$

where f_n is the volume fraction of the nth component. For dry ammonium nitrate and ammonium sulfate the value $m_{\mathrm{dry}} = 1.53$ is used as refraction index [*Toon and Pollak*, 1976], for water the value is $m_{\mathrm{H_2O}} = 1.33$ [*Hale and Querry*, 1973]. For the soot particles recent wavelength-dependent measurements of the refraction index of diesel soot made in the AIDA chamber are used [*Kamm et al.*, 1999; *Schnaiter et al.*, 2003] as listed in Table 3. Since for these measurements "real" diesel soot was used, the refraction indices used for

Table 3. Refraction Index of Diesel Soot Depending on the Wavelength λ[a]

λ, nm	m_s
280	1.30 + i0.59
300	1.31 + i0.59
320	1.33 + i0.60
350	1.34 + i0.61
400	1.38 + i0.62
450	1.41 + i0.64
500	1.45 + i0.66
550	1.49 + i0.67
600	1.51 + i0.69
700	1.57 + i0.73

[a]*Schnaiter et al.* [2003].

our study implicitly account for the fact that soot particles in the atmosphere also contain organic carbon.

[31] The extinction coefficient for the whole aerosol population is given by the sum of the extinction coefficients of the individual modes. Moreover, the soot-containing particles are assumed to consist of an insoluble core and a soluble shell where the core is centered. The integral in equation (10) is solved using a Gauss-Hermite method. With the procedure described in this section a three dimensional distribution of extinction coefficients can be calculated for every point in time. These data serve in the following as input data for the radiative transfer calculations.

2.4. STAR

[32] The radiation transfer calculations are carried out offline with the radiation model STAR (System for Transfer of Atmospheric Radiation). In KAMM/DRAIS STAR is employed to calculate the photolysis rates for 21 photochemical relevant gases. This model was developed by *Ruggaber et al.* [1994] on the basis of the one-dimensional spectral radiation transfer model by *Nakajima and Tanaka* [1986], which calculates vertical profiles of spectral irradiance and spectral actinic flux by a matrix operator method for the wavelength interval from 280 nm to 700 nm. Within this interval the radiative fluxes are calculated at 24 wavelengths. The optical properties are calculated for 10 wavelengths (compare Table 3) and interpolated linearly in between.

[33] Input data are vertical profiles of the optical thickness, single scattering albedo (e.g., the ratio of scattering and extinction coefficient) and the phase functions where contributions of gases, aerosol and clouds can be considered.

[34] So far, concerning the contribution of the aerosol particles, standard profiles by *d'Almeida et al.* [1991] have been used. For the following investigations, these standard profiles are replaced within the boundary layer by profiles calculated with KAMM/DRAIS for the situation described below. For every grid point and wavelength interval extinction, scattering, absorption coefficients and a mean phase function are calculated as described in section 2.3. In addition, the modeled vertical profiles of the absorbing trace gases NO_2 and O_3 and of the meteorological parameters (pressure, temperature, specific humidity) are considered. The albedo is set to 0.2 for all grid points. The radiation transfer calculations are carried out one-dimensionally for each column of the model domain.

2.5. Topography and Meteorological Conditions

[35] The model is applied to an area in southwestern Germany. It covers main parts of Baden-Württemberg and the adjacent regions (Figure 2).

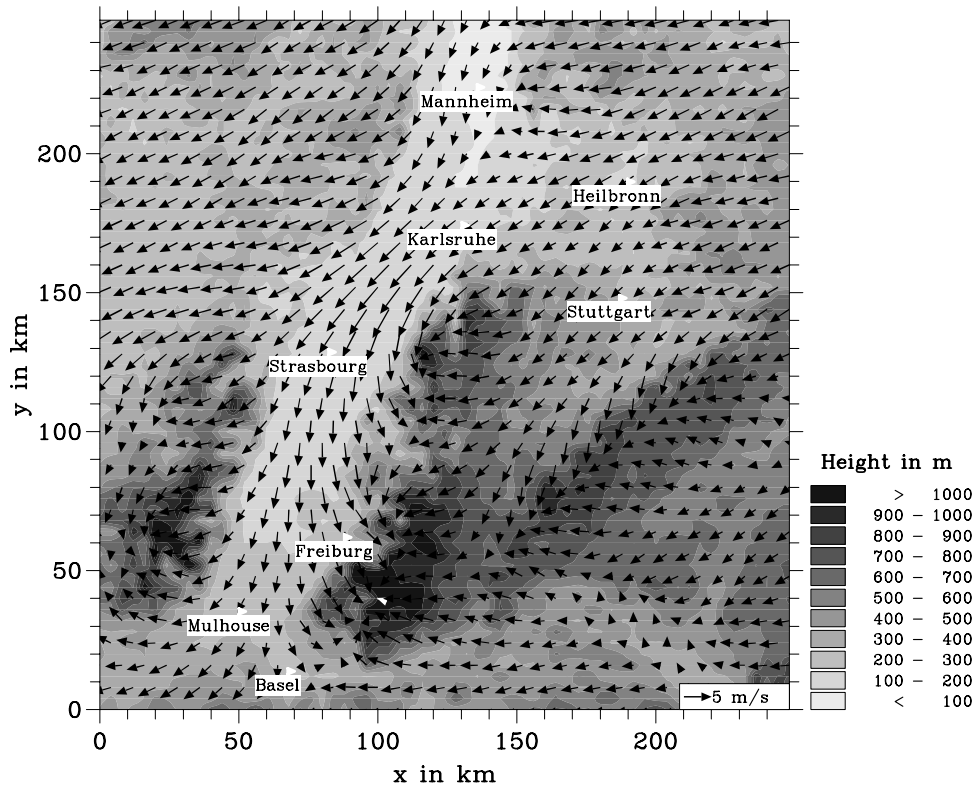

Figure 2. Topography of the model domain and wind field at 20 m above the surface at 1200 CET.

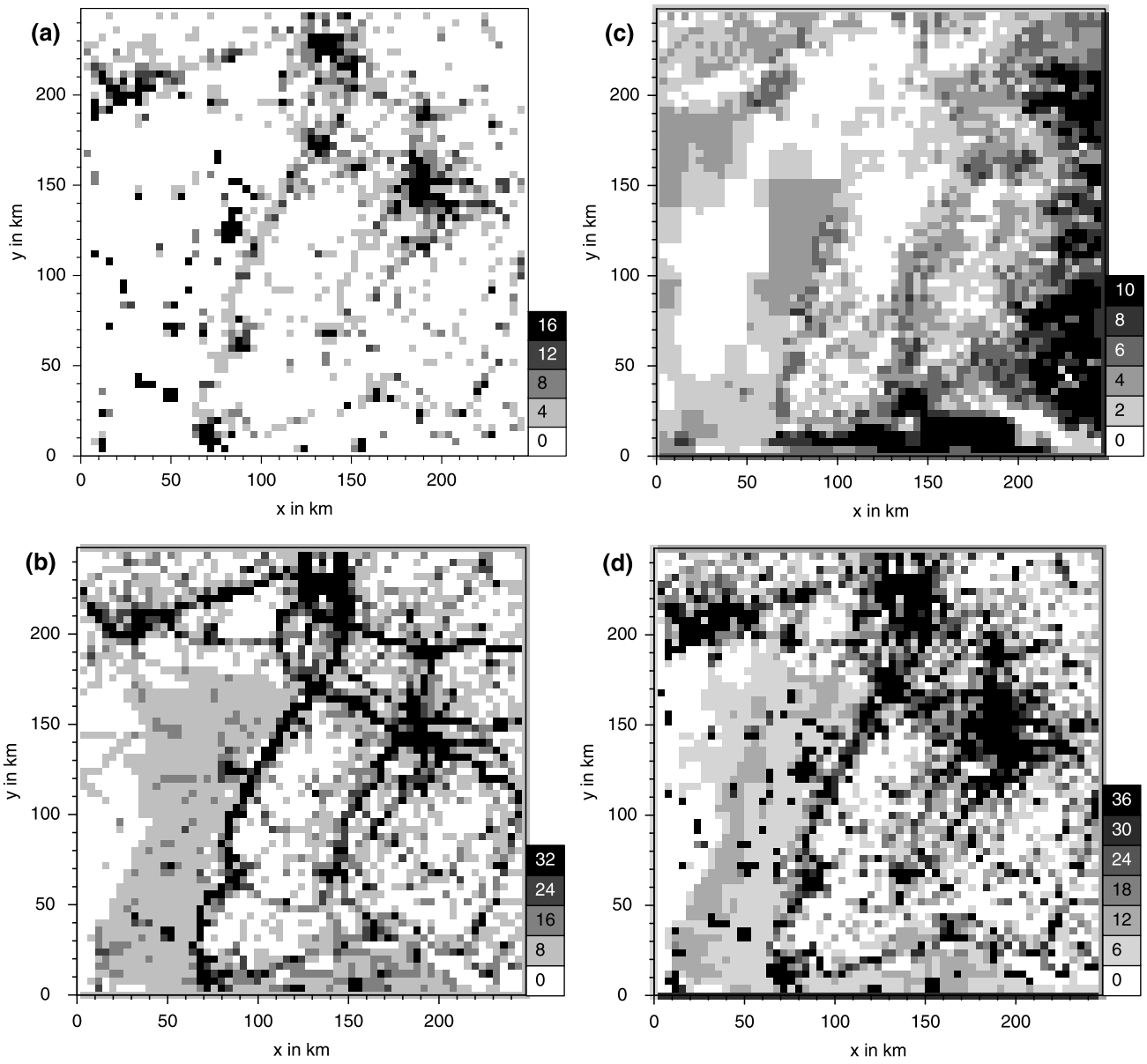

Figure 3. Horizontal distributions of the emissions of (a) SO_2, (b) NO_x, (c) NH_3, and (d) VOC at 0800 CET. Numbers are given for areas of 4×4 km^2 in kg h^{-1}.

[36] The terrain height differs from 110 m in the Rhine valley up to 1500 m in the southern part of the Black Forest and the Vosges mountains. The horizontal grid size used for our simulations is 4×4 km^2. The model domain covers an area of 248×248 km^2. A typical summer situation is simulated with a geostrophic wind of 4.5 m s^{-1} blowing from East. The solar radiation and the photolysis rate coefficients are calculated corresponding to July 3.

2.6. Emissions

[37] To carry out the simulations, data for the anthropogenic emissions are necessary. The anthropogenic emissions of SO_2, CO, NO_x, NH_3, 32 individual classes of VOC according to the RADM2 mechanism and diesel soot emissions were precalculated with a spatial resolution of 4×4 km^2 and a temporal resolution of one hour. The anthropogenic gas phase emission data account for traffic emissions, emissions by large point sources and area sources such as households and industrial areas and represent summer conditions. The diesel soot emissions represent the sources by traffic. The method used to determine these emissions is described by *Obermeier et al.* [1995], *Wickert et al.* [1999], *Pregger et al.* [1999], and *Seier et al.* [2000]. The biogenic emissions were calculated online as described above. Additionally to the source strength, the median diameter and the standard deviation of the distribution of the emitted soot particles must be prescribed. According to measurements by *Vogt et al.* [2000] the median diameter of the emitted soot particles is fixed to 60 nm and the standard deviation to 1.8. Figures 3–4 show the horizontal distributions of the emissions of SO_2, NO_x, NH_3, biogenic and anthropogenic VOC and diesel soot at 0800 CET. While the emissions of SO_2, NO_x and soot reflect the locations of the urban areas and highways, the NH_3 emissions are concen-

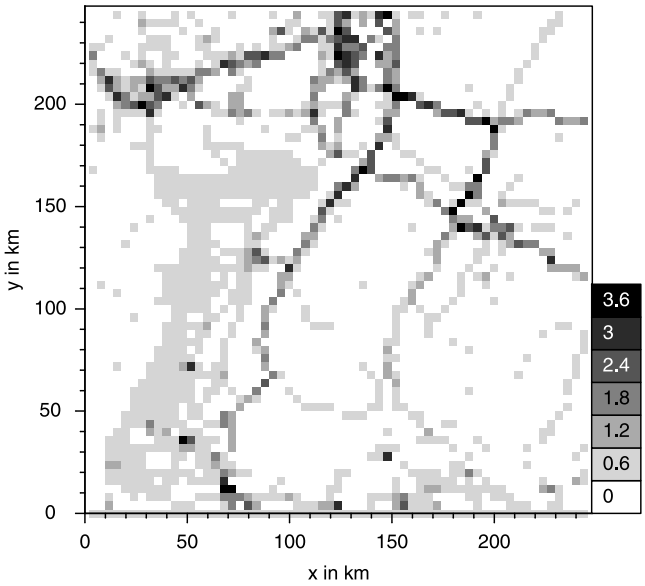

Figure 4. Horizontal distributions of the diesel soot emissions, at 0800 CET. Numbers are given for areas of 4×4 km^2 in kg h^{-1}.

trated in the rural areas of the model domain since they originate mainly from agricultural activities.

2.7. Initialization

[38] The initialization of the aerosol phase is done in the following manner: For the first four hours of the simulation the gas phase is running without the aerosol phase. After four hours the existing amount of H_2SO_4 is distributed between the modes $\mathbf{i_f}$, $\mathbf{j_f}$, $\mathbf{i_c}$, $\mathbf{j_c}$ so that 98% of the amount of H_2SO_4 is assigned to the accumulation modes $\mathbf{j_f}$, $\mathbf{j_c}$ and 2% to the Aitken modes $\mathbf{i_f}$, $\mathbf{i_c}$. The other aerosol constituents are initialized with a minimum value and are brought to equilibrium in the following time step. Since the geometric standard deviation is fixed, the number density in each mode can be calculated if the median diameter is prescribed for the initial step. These values are given in Table 4.

3. Results

[39] On the basis of the simulated distributions of the tropospheric aerosol particles we derive the impact of aerosol particles on the downward radiative flux in southwest Germany for a typical summer day. Before the outcome of the sensitivity studies concerning this focus will be discussed, we present selected results of the simulation with respect to the meteorological conditions, the distribution of the gas and aerosol phase species and the extinction coefficients.

3.1. Meteorology

[40] Figure 2 shows the wind field as it is predicted at 20 m above the surface at 1200 CET. The characteristics of the wind field are the channeling of the airflow in the Rhine Valley and the thermal secondary flow systems on the slopes of the mountains. The maximum temperature in the Rhine Valley reaches about 28°C. The relative humidity in the lowest model layer varies between 55% and 90% during the night and between 40% and 60% during daytime.

3.2. Gas Phase

[41] Figure 5 shows the horizontal distributions of the precursor species for the secondary aerosol particles, SO_2, NH_3 and HNO_3, respectively, at 20 m above the surface at 1200 CET. The plumes downwind of the urban centers of Karlsruhe, Strasbourg, Mannheim and Saarbrücken can be identified in the distribution of the SO_2 concentration. At some grid points concentrations of 30 ppb are reached. However, in the largest part of the model area the values range below 5 ppb. The distribution of the NH_3 concentration likewise reflects the distribution of the sources (compare Figure 3c). The maximum concentrations amount to 9 ppb. In the northwestern part of the model domain ammonium is almost exclusively present in the particle phase therefore the gas phase concentrations of NH_3 are very low. As a species which is formed by photochemical processes, HNO_3 shows high concentrations in the plumes of Saarbrücken and Mannheim as well as in the Rhine Valley and in the region of Lake Constance.

3.3. Particle Phase

[42] Figure 6 shows the horizontal distributions of sulfate, ammonium and nitrate at 20 m above the surface at 1200 CET. Here, the total dry mass concentrations, summed over the modes $\mathbf{i_f}$, $\mathbf{j_f}$, $\mathbf{i_c}$, and $\mathbf{j_c}$ are presented. Low sulfate concentrations are found in the mountainous regions, the highest concentrations are found in the Rhine Valley, since the emissions of SO_2 from the urban centers Mannheim/Heidelberg, Karlsruhe and Strasbourg accumulate in this area. High sulfate concentrations are also found in the southeastern part of the model domain where individual point sources exist. Overall, the gradients of the sulfate concentrations are small in the model domain. This finding is explained by the fact that in the plumes of the urban centers where the SO_2 concentrations are high also the NO_x concentrations reach high values whereas the OH concentrations are low. In the rural areas, the OH concentrations are higher, but the SO_2 concentrations are low. This leads to a rather uniformly distributed H_2SO_4 production, and therefore sulfate is distributed uniformly in the model domain as well.

[43] The distribution of the ammonium concentrations reflects both the pattern of the ammonia emissions and of the sulfate distribution since most of the ammonium is present as ammonium sulfate. Accordingly, the ammonium concentration is low in the northwestern part of the model domain. In the Rhine Valley the ammonium concentrations are not high enough to neutralize the available sulfate.

[44] Under the considered situation, even at those points where the sulfate is neutralized, ammonium nitrate forma-

Table 4. Median Diameters of the Five Modes for the Initialization

	d_{gi}, μm
$d_{gi_f,\mathrm{ini}}$	0.01
$d_{gj_f,\mathrm{ini}}$	0.07
$d_{gi_c,\mathrm{ini}}$	0.01
$d_{gj_c,\mathrm{ini}}$	0.07
$d_{gs,\mathrm{ini}}$	0.05

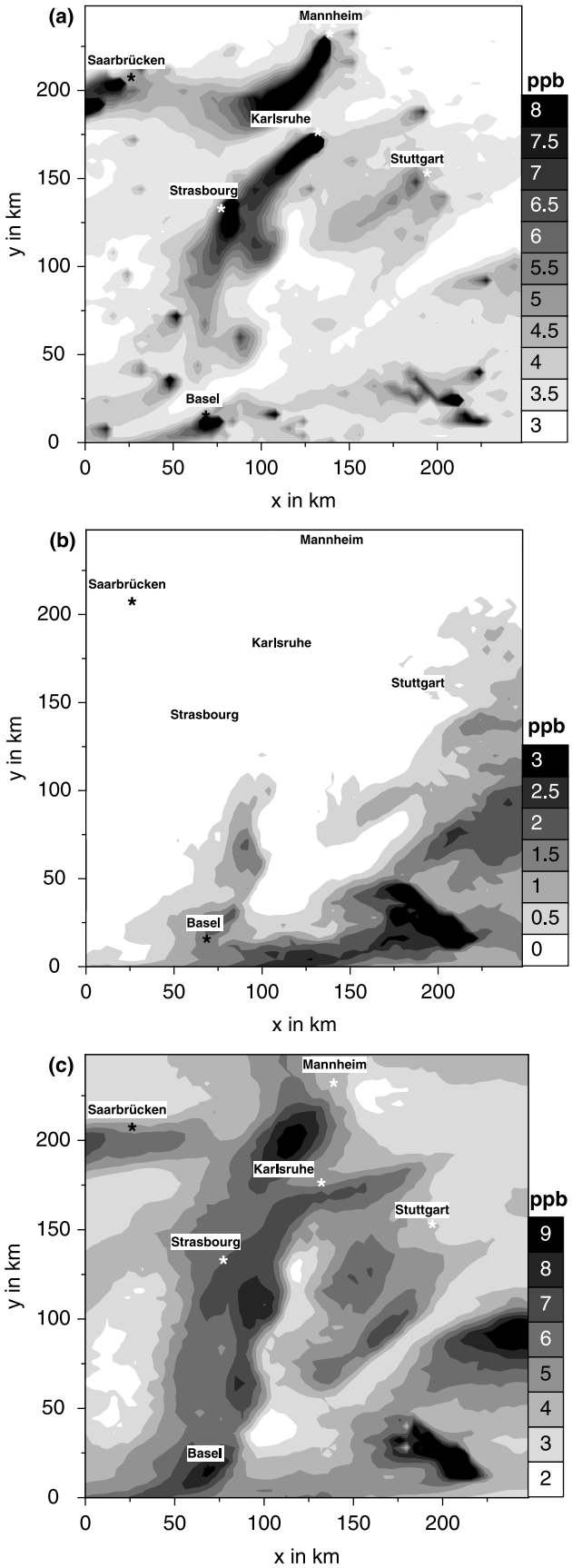

Figure 5. Horizontal distribution of (a) the SO_2 concentration, (b) the NH_3 concentration, and (c) the HNO_3 concentration at 20 m above the surface at 1200 CET.

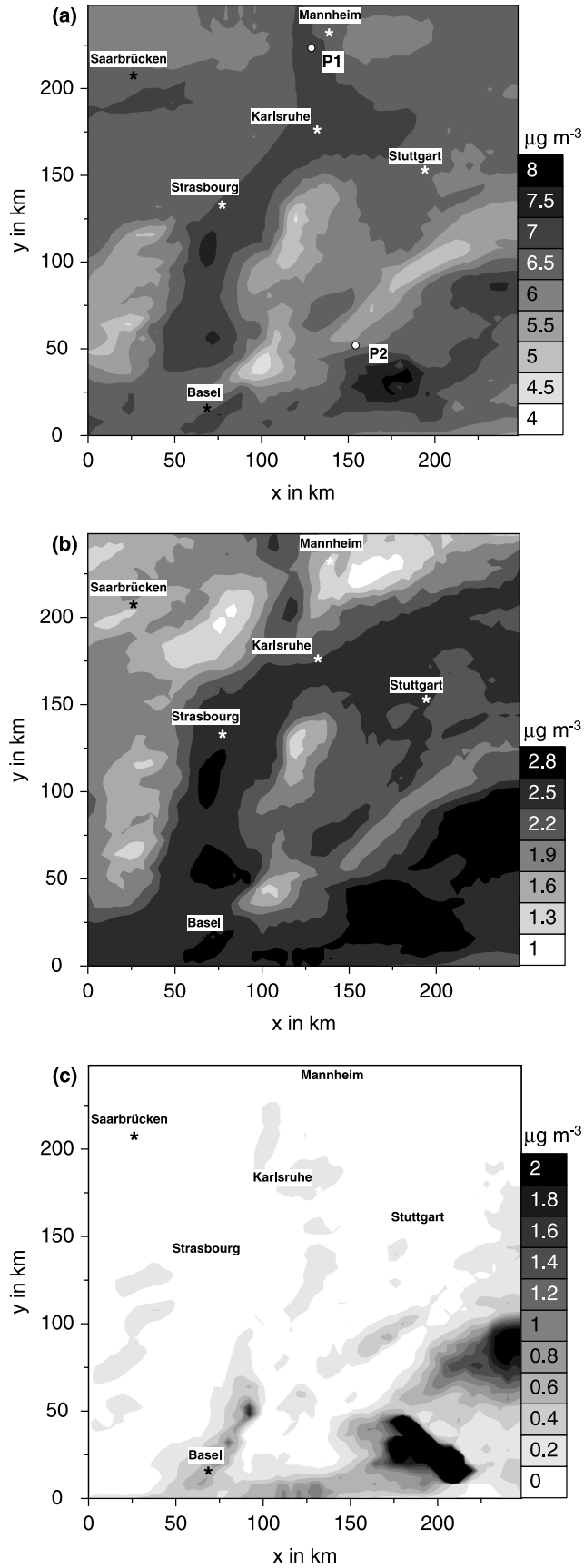

Figure 6. Horizontal distribution of (a) the SO_4^{2-} mass density, (b) the NH_4^+ mass density, and (c) the NO_3^- mass density at 20 m above the surface at 1200 CET.

tion is not favored because of the high temperatures. This behavior is well documented by several authors [e.g., *Mehlmann and Warneck*, 1995; *Possanzini et al.*, 1999; *Schaap et al.*, 2002]. Only in the area of Lake Constance ammonium nitrate is present in the afternoon because of the temperature inversion over the water surface.

[45] Figure 7 shows the horizontal distribution of the soot concentration. We distinguish between internally mixed (soot in the modes $\mathbf{i_c}$ and $\mathbf{j_c}$) and externally mixed soot. The distribution of the externally mixed soot reflects the distribution of the sources, whereas in the plumes of the urban areas soot is present in the internal mixture.

[46] Also the vertical distribution shows that soot in the external mixture is limited to the immediate vicinity of the sources. Figure 8 shows a vertical section for y = 80 km. In the elevated layers, soot exclusively exists internally mixed.

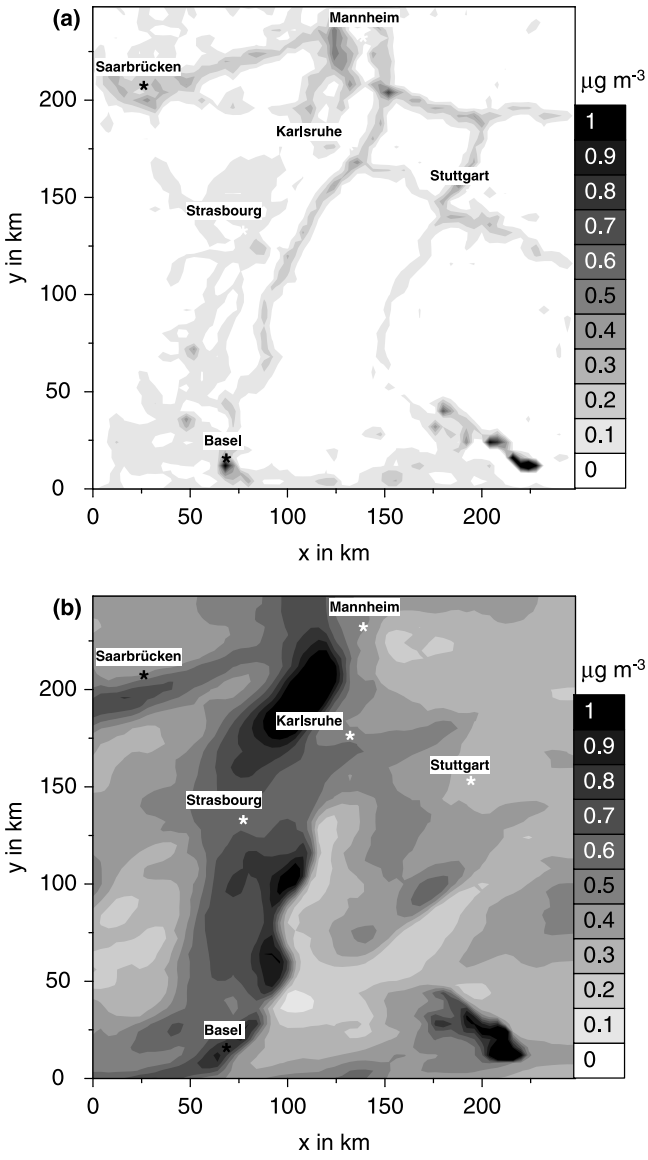

Figure 7. Horizontal distribution of (a) the externally mixed diesel soot mass density and (b) the internally mixed diesel soot mass density at 20 m above the surface at 1200 CET.

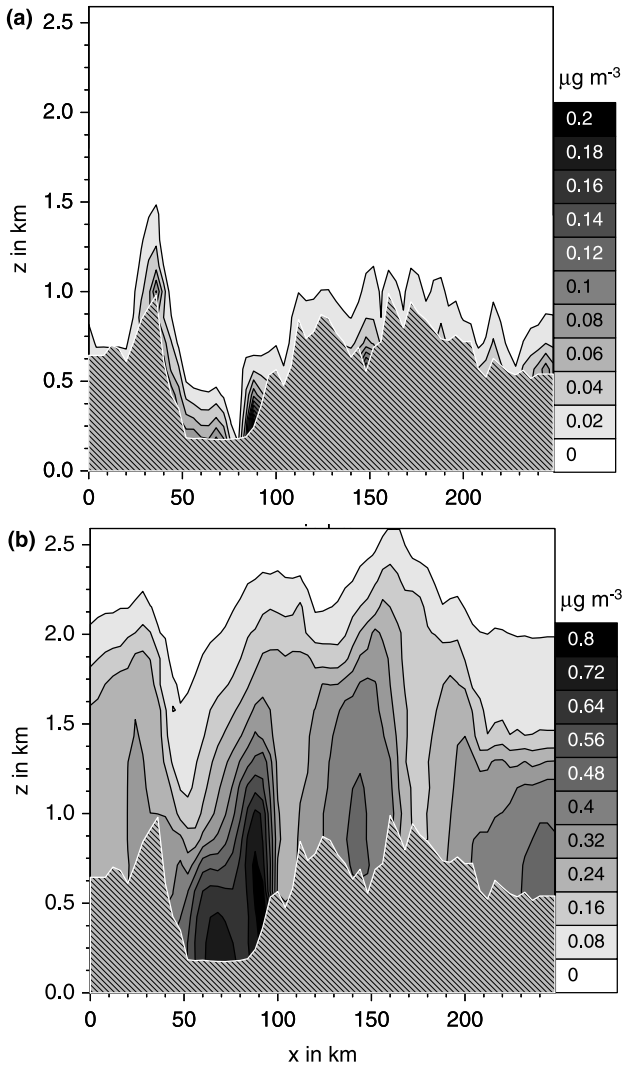

Figure 8. Vertical distribution of (a) the externally mixed diesel soot mass density and (b) the internally mixed diesel soot mass density at y = 80 km at 1200 CET.

[47] Overall, the maximum mass concentration of total dry aerosol at the given time reaches 13 μg m^{-3} in the Rhine Valley where the main constituent is sulfate and 35 μg m^{-3} in the area of the Lake Constance where ammonium nitrate is present.

[48] Figure 9 shows the daily cycle of the individual aerosol species together with the total dry aerosol mass concentration for two different grid points 20 m above the surface. Both points are marked in Figure 6a. The first point (P1) is the city of Mannheim and therefore exposed to an urban environment. As a species which is produced photochemically the sulfate concentration peaks in the afternoon reaching a value of 7.5 μg m^{-3}. Although HNO_3, the precursor of nitrate, also reaches its maximum in the afternoon, the highest nitrate concentrations occur in the early morning with 2.3 μg m^{-3}. This behavior is characteristic for summer conditions [*Mehlmann and Warneck*, 1995; *Possanzini et al.*, 1999], since ammonium nitrate is not stable because of the high temperatures in the afternoon. The diurnal cycle of the aerosol water displays a

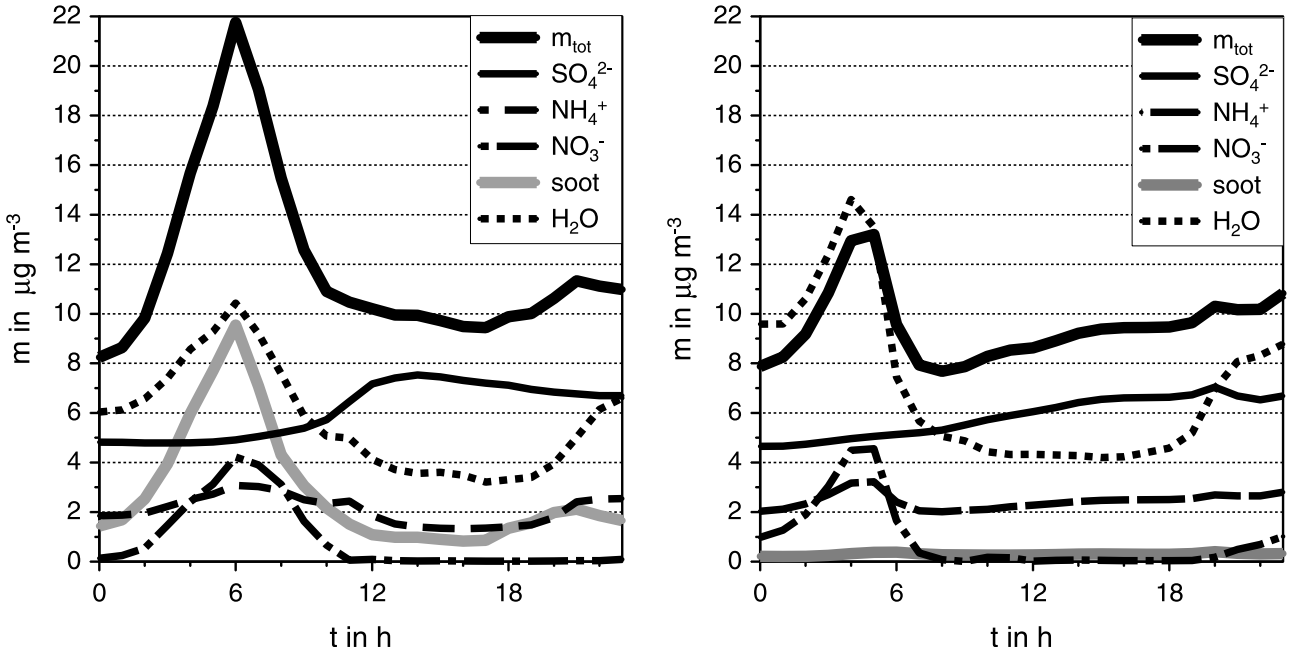

Figure 9. Daily cycle of the different aerosol species and the total dry aerosol mass for the grid points P1 (left) and P2 (right). See text for details.

maximum in the morning as well, since the relative humidity is highest at this time of the day. The evolution of the soot concentration shows also a maximum in the morning which is caused by high traffic emissions accumulating in a shallow boundary layer. The maximum concentration is 9.8 μg m^{-3}, which demonstrates the urban influence. A second maximum is reached in the evening, which is also related to traffic emissions, but less pronounced, because the emissions are released in a larger volume. The qualitative evolution of the diurnal cycle of the soot concentration is confirmed by measurements by *Allen et al.* [1999] and *Brunnemann et al.* [1996]. The second point (P2) is situated in a rural environment. Here, the soot concentrations are considerably lower, because this location is further away from the main traffic routes. The diurnal cycle is not as pronounced as it is the case for P1, however, there are still two maxima detectable where the maximum concentration reaches 0.4 μg m^{-3}. The other species show similar diurnal cycles and concentration levels to the first location. At both sites, the water content shows a minimum in the afternoon where the maximum values at P2 exceed the ones at P1 during the night. The simulated concentrations of the aerosol species compare well both in respect of magnitude and diurnal cycle with measurements made in Continental Europe [*Neusüß et al.*, 2002; *Zappoli et al.*, 1999; *Mészáros et al.*, 1997; *Van Dingenen et al.*, 2002].

[49] A comparison to measurement data would be desirable, however, for our model domain detailed data of the aerosol composition are not yet available. To give some comparison anyway, Table 5 is compiled in which the model results and results of measurement campaigns carried out in Central Europe are listed. For the model results the 24-hour-average value is calculated for each grid point at the ground. The minimum and the maximum of these values is given in Table 5. To give an idea of the range of the values over the course of a day also the absolute maximum

Table 5. Overview of Calculated Particle Concentrations and Measurements in Central Europe

Measured, μg m^{-3}	Station	Period	Data Reference
Sulfate (*Modeled Concentrations: 5.0/7.1 and 3.7/9.4*)[a]			
3.5	Lindenberg	July	*Neusüß et al.* [2002]
7.6	K-Puszta	July–August	*Zappoli et al.* [1999]
6.1	K-Puszta	summer	*Mészáros et al.* [1997]
9.7	Deuselbach	June (afternoon)	*Mehlmann and Warneck* [1995]
4.3	Manndorf	July (daytime)	*Possanzini et al.* [1999]
2–20	Vinon	June	*Van Dingenen et al.* [2002]
Nitrate (*Modeled Concentrations: 0.07/6 and 0.0/11*)[a]			
0.9	Lindenberg	July	*Neusüß et al.* [2002]
1.9	K-Puszta	July–August	*Zappoli et al.* [1999]
1.2	K-Puszta	summer	*Mészáros et al.* [1997]
0.7	Deuselbach	June (afternoon)	*Mehlmann and Warneck* [1995]
0.3–2.5	Vinon	June	*Van Dingenen et al.* [2002]
Ammonium (*Modeled Concentrations: 1.3/5.9 and 0.9/10.1*)[a]			
1.4	Lindenberg	July	*Neusüß et al.* [2002]
2.5	K-Puszta	July–August	*Zappoli et al.* [1999]
2.5	K-Puszta	summer	*Mészáros et al.* [1997]
1.7	Manndorf	July (daytime)	*Possanzini et al.* [1999]
2.5	Deuselbach	June (afternoon)	*Mehlmann and Warneck* [1995]
1.5–3	Vinon	June	*Van Dingenen et al.* [2002]
Soot (*Modeled Concentrations: 0.2/3.5 and 0.1/9.3*)[a]			
1.3	Lindenberg	July	*Neusüß et al.* [2002]
0.6	K-Puszta	July–August	*Zappoli et al.* [1999]
2.6	Vienna	summer	*Hitzenberger and Tohno* [2001]
1.5	Vinon	June	*Van Dingenen et al.* [2002]

[a]The first set of values is the minimum/maximum of the average value over 24 hours, and the second set of values is the absolute minimum/maximum in the model domain. Modeled concentrations are given in μg m^{-3}.

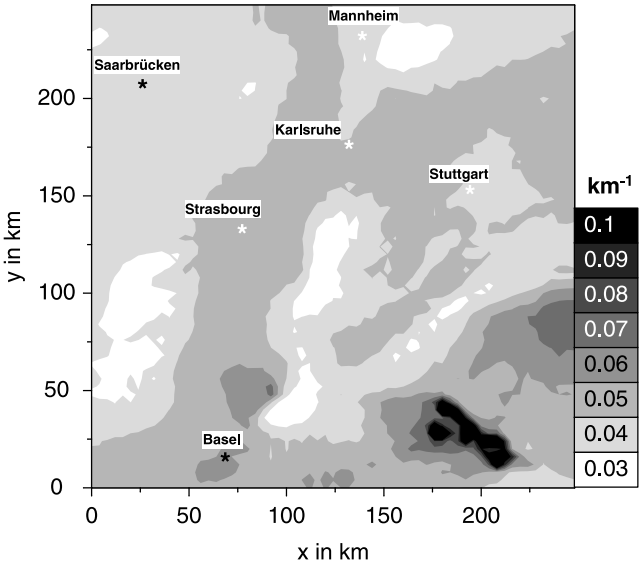

Figure 10. Horizontal distribution of the extinction coefficient at 20 m above the surface at 1200 CET.

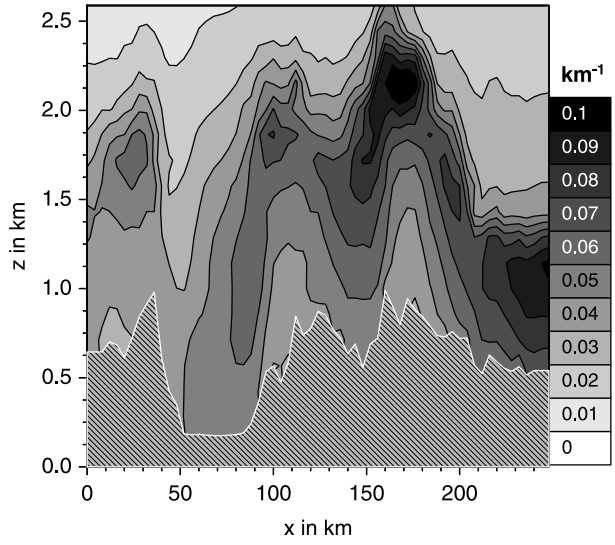

Figure 11. Vertical distribution of the extinction coefficient at y = 80 km at 1200 CET.

and minimum values are listed in italics. It shows that our model results are within the range of the measured data.

3.4. Extinction Coefficients

[50] Figure 10 shows the horizontal distribution of the extinction coefficient for the wavelength of 550 nm 20 m above the surface at 1200 CET. The highest values in this layer occur in the area of the Lake Constance where ammonium nitrate aerosol is present and also the water content of the aerosol is high. Hence the particles grow to a size where they effectively scatter light.

[51] For a comparison, Table 6 gives measured absorption, scattering and extinction coefficients. It shows that the calculated values are in a range which is representative for a moderately polluted summer conditions in central Europe [*Wex et al.*, 2002; *Hess et al.*, 1998].

[52] Figure 11 presents a vertical section of the extinction coefficients for y = 80 km and 1200 CET. The extinction coefficients increase with height because of the increasing water content of the particles. This in turn is due to increasing relative humidity with height. Lidar measurements [*Carnuth and Trickl*, 2000] confirm qualitatively this vertical distributions of the extinctions coefficient simulated with KAMM/DRAIS.

[53] From the calculated volume absorption coefficients the specific absorption coefficient of soot α can be derived. The specific absorption coefficient α is given by the volume absorption coefficient b_a divided by the mass density of soot m_s in the respective mode

$$\alpha = \frac{b_a}{m_s}. \tag{14}$$

[54] Figure 12 shows the frequency distribution of the specific absorption for the modes **s**, $\mathbf{i_c}$ and $\mathbf{j_c}$ for all grid points in the model domain. It is obvious that higher values are reached for the internally mixed soot. The range of values is in good agreement with *Fuller et al.* [1999].

3.5. Impact on Radiation

[55] In this section we investigate the impact of the aerosol particles on the global radiation at the ground. Using the radiative transfer model STAR as described above, we calculate the irradiance F_d integrated of the wavelength interval from 290 nm to 700 nm at ground level for three cases. For case 1 the radiative calculations are based on the aerosol distribution which were presented in section 3.3. In case 2 the boundary layer is considered to be completely free of aerosols. In case 3 the refraction index of the soot component in modes $\mathbf{i_c}$, $\mathbf{j_c}$ and **s** is artificially modified and set equal to the values of the soluble material. the particles are retained in case 3, only the refraction index changes.

[56] The results of case 1 are displayed in Figure 13a. The values for F_d vary between 455 and 476 W m^{-2}. This

Table 6. Overview of Measured Scattering, Absorption, and Extinction Coefficients

	Measured, km^{-1}	Station	Period	Data Reference
b_s	0.01–0.08	Lindenberg, ground station	July–August	*Wex et al.* [2002]
b_s	0.01–0.08	Lindenberg, vertical profile	August	*Wex et al.* [2002]
b_a	0.004–0.025	Lindenberg, ground station	July–August	*Wex et al.* [2002]
b_a	0.015–0.03	South of Italy	June–July	*Horvath* [1996]
b_e	0.026	"Continental clean"		*Hess et al.* [1998]
b_e	0.075	"Continental average"		*Hess et al.* [1998]
b_e	0.175	"Continental polluted"		*Hess et al.* [1998]
b_e	0.353	"Urban"		*Hess et al.* [1998]
b_e	0.03–0.2	South of Italy	June–July	*Horvath* [1996]

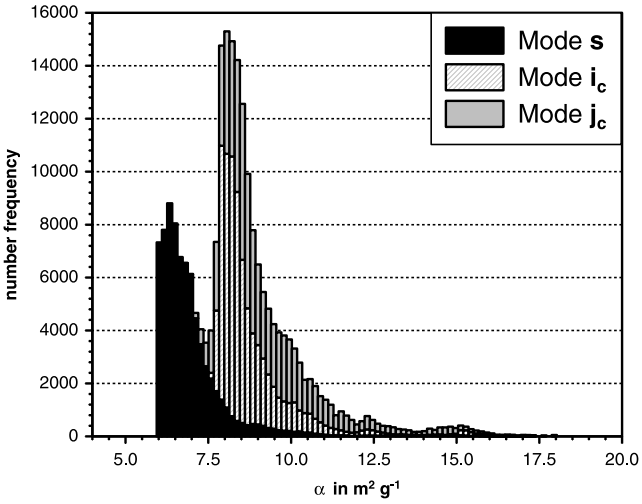

Figure 12. Frequency distribution of the specific absorption of soot for all grid points in the model domain.

variance can partially be attributed to the change in terrain height resulting in a varying thickness of the optical path. In addition, the spatial distribution of the trace gases and the spatial distribution of the aerosol cause a variance of F_d. The latter can be seen if one follows the distribution of F_d along the Rhine Valley where the terrain height is almost constant and F_d still varies between 455 and 467 W m^{-2}. The overall impact of the aerosol particles in the boundary layer can be quantified by calculating F_d without aerosol (case 2). Figure 13b shows the differences between case 2 and case 1 (ΔF_{d21}). The highest differences occur in the Rhine Valley (25 W m^{-2}) and in the area of the Lake Constance (22 W m^{-2}) where a high aerosol load was calculated (Figures 6–7). These differences in F_d correspond to an aerosol forcing (effect of aerosol on the net (down minus up) solar flux) at the surface of up to -20 W m^{-2}.

[57] In recent literature, the impact of aerosols on the downward flux of solar radiation at the surface and the aerosol forcing at the surface has been derived from measurements for several campaigns. *Markowicz et al.* [2002] find a diurnal average reduction of 17.9 W m^{-2} in the surface solar radiation for the MINOS experiment at the Finokalia sampling station in Crete (Greece). *Ramanathan et al.* [2001] report a regional forcing in the Indian Ocean region of about -15 to -25 W m^{-2} at the surface. *Russell et al.* [2002] present a change in the downward flux of solar radiation for the North Pacific during the ACE-Asia campaign of -20 to -40 W m^{-2} due to the aerosol load. For the ESCOMPTE campaign a radiative forcing of -33 W m^{-2} is derived for the station Vallon Dol [*Cachier et al.*, 2002].

[58] Given that for most of these measurement campaigns the conditions were more heavily polluted compared to the conditions in southwest Germany, our results based on the simulated aerosol distributions fit well in the picture. A modeling study by *Jacobson* [1997b] for the area of Los Angeles shows that aerosols containing soot reduce peak downward solar radiation by 55 W m^{-2}. This value differs from our finding by the factor of two which can be explained by several reasons. First, our study does not include the whole solar spectrum and second, the aerosol load is lower in our study. Further studies have shown, however, that the fine particles impact mainly the wavelengths below 700 nm, this means that the second reason is more important in our case. Third, the contribution of the coarse mode is not considered in our case.

[59] The impact of soot is quantified by case 3. Figure 13c (bottom) shows the differences between case 3 and case 1 (ΔF_{d31}). The maximum difference is now 8 W m^{-2}, which is about 30% of the effect caused by the aerosol overall. Figure 13d shows the ratio of the differences between case 3 and 1 and case 2 and 1. The higher these values the more important is the impact of soot. The highest values are reached in the plume of Mannheim and in the Rhine Valley. Considering that soot only contributes less than 10% to the total dry aerosol mass in these areas, this result shows that soot is a very important constituent of the tropospheric aerosol, even under only moderately polluted conditions as they prevail in southwest Germany.

4. Conclusions

[60] The aerosol model MADE [*Ackermann et al.*, 1998; *Schell et al.*, 2001] was extended for the treatment of soot particles. MADEsoot now accounts for the species sulfate, nitrate, ammonium, water and soot. Two ageing processes which transfer soot form external into internal mixture are taken into account. The first one is the condensation of sulfuric acid, the second one is the coagulation of pure soot particles with soot free and soot containing particles, respectively.

[61] We carried out model simulations with the comprehensive model system KAMM/DRAIS to quantify the impact of aerosol particles on global radiation. The model system was applied to a summer situation in the southwestern part of Germany. The results show that externally mixed soot only occurs in the vicinity of the sources. At 1200 CET the soot concentrations in the model domain reach about 1 μg m^{-3}. The total dry aerosol mass reaches 12 μg m^{-3} in the Rhine valley and 30 μg m^{-3} in the area of the Lake Constance where nitrate formation takes place. In most of the model domain, however, nitrate formation is not favored during the daytime. These values are in the range of recent observations.

[62] On the basis of the simulated aerosol distributions the optical properties of the aerosol were derived using Mie calculations. The extinction coefficients exhibit a pronounced spacial variation. At 1200 CET the values for the extinction coefficient for the wavelength of 550 nm vary at ground level between 0.03 km^{-1} in the Black Forest and the Vosges Mountains and 0.24 km^{-1} in the area of the Lake Constance. Moreover, the values or the extinction coefficients increase with height since the relative humidity increases with height as well which leads to a growth of the aerosol particles.

[63] The results of the radiative transfer calculations show that for the presented case, the aerosol in the boundary layer reduces the downward flux of the solar radiation, integrated over the wavelength interval from 280 nm to 700 nm, by up to 25 W m^{-2}, which corresponds to a decrease of 5%. These findings are confirmed by the results of recent measurement campaigns. Sensitivity studies have shown that up to 50%

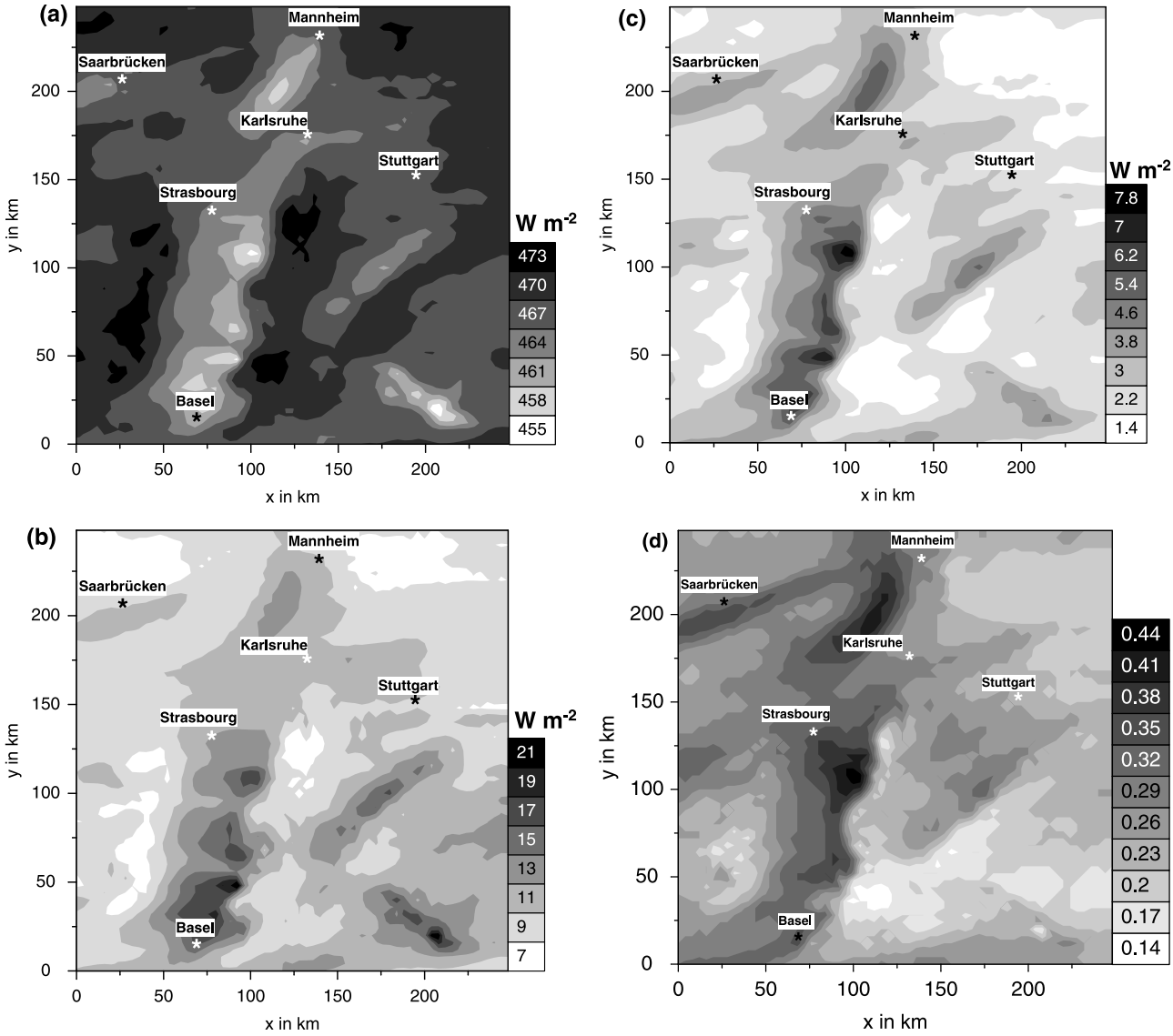

Figure 13. (a) Horizontal distribution of the downward flux of solar radiation (280 nm–700 nm) at ground level at 1200 CET, (b) horizontal distribution of ΔF_{d21}, (c) horizontal distribution of ΔF_{d31}, and (d) horizontal distribution of the ratio of ΔF_{d31} and ΔF_{d21}.

of the effect can be attributed to the impact of soot. This demonstrates the strong impact of soot on global radiation even under moderately polluted conditions.

References

Ackerman, T., and O. Toon, Absorption of visible radiation in atmosphere containing mixtures of absorbing and nonabsorbing particles, *Appl. Opt.*, *20*, 3661–3667, 1981.

Ackermann, I., H. Hass, M. Memmesheimer, A. Ebel, F. Binkowski, and U. Shankar, Modal aerosol dynamics model for Europe: Development and first applications, *Atmos. Environ.*, *32*, 2981–2999, 1998.

Adrian, G., and F. Fiedler, Simulation of unstationary wind and temperature fields over complex terrain and comparison with observations, *Beitr. Phys. Atmos.*, *64*, 27–48, 1991.

Allen, G., J. Lawrence, and P. Koutrakis, Field validation of a semi-continuous method for aerosol black carbon (aethalometer) and temporal patterns of summertime hourly black carbon measurements in southwestern PA, *Atmos. Environ.*, *33*, 817–823, 1999.

Bär, M., and K. Nester, Parameterization of trace gas dry deposition velocities for a regional mesoscale diffusion model, *Ann. Geophys.*, *10*, 912–923, 1992.

Binkowski, F., and U. Shankar, The regional particulate matter model: 1. Model description and preliminary results, *J. Geophys. Res.*, *100*, 26,191–26,209, 1995.

Bohren, C., and D. Huffman, *Absorption and Scattering of Light by Small Particles*, John Wiley, Hoboken, N. J., 1983.

Boucher, O., and T. Anderson, General circulation model assessment of the sensitivity of direct climate forcing by anthropogenic sulfate aerosols to aerosol size and chemistry, *J. Geophys. Res.*, *100*, 26,117–26,134, 1995.

Brüggemann, E., et al., Korngrößendifferenzierte Identifikation der Anteile verschiedener Quellgruppen an der Feinstaubbelastung, *Abschlussber. 13-8802.3521/46*, Sächsisches Landesamt für Umwelt und Geol., Freiberg, Germany, 2000.

Brunnemann, G., L. Kins, and R. Dlugi, Physical and chemical characterization of the atmospheric aerosol: An overview of the measurements during the SANA 2 campaign at Melpitz, *Meteorol. Z. N. F.*, *5*, 245–256, 1996.

Busen, R., and G. Hänel, Radiation budget of the boundary layer. Part I: Measurement of absorption of solar radiation by atmospheric particles and water vapor, *Beitr. Phys. Atmos.*, *60*, 229–240, 1987.

Cachier, H., et al., Aerosol studies during the ESCOMPTE experiment: An overview, paper presented at Joint CACGP/IGAC 2002 International Symposium, Comm. on Atmos. Chem. and Global Pollut., Crete, Greece, 2002.

Carnuth, W., and T. Trickl, Transport studies with the IFU three-wavelength aerosol lidar during VOTALP Mesolcina experiment, *Atmos. Environ.*, *34*, 1425–1434, 2000.

Charlson, R., J. Langner, H. Rohde, C. Leovy, and S. Warren, Pertubation of the Northern Hemisphere radiative balance by backscattering from anthropogenic sulphate aerosols, *Tellus, Ser. A-B*, *43*, 152–163, 1991.

Chung, S., and J. Seinfeld, Global distribution and climate forcing of carbonaceous aerosols, *J. Geophys. Res.*, *107*(D19), 4407, doi:10.1029/2001JD001397, 2002.

Cooke, W., and J. Wilson, A global black carbon aerosol model, *J. Geophys. Res.*, *101*, 19,395–19,408, 1996.

Corsmeier, U., et al., Ozone and PAN formation inside and outside of the Berlin plume: Process analysis and numerical process simulation, *J. Atmos. Chem.*, *42*, 289–322, 2002.

d'Almeida, G., P. Koepke, and E. Shettle, *Atmospheric Aerosols Global Climatology and Radiative Characteristics*, A. Deepak, Hampton, Va., 1991.

Dorwarth, G., Numerische Berechnung des Druckwiderstandes typischer Geländeformen, Ph.D. thesis, Inst. für Meteorol. und Klimaforsch. der Univ. Karlsruhe (TH), Karlsruhe, Germany, 1985.

Fassi-Fihri, A., K. Suhre, and R. Rosset, Internal and external mixing in atmospheric aerosols by coagulation: Impact on the optical and hygroscopic properties of the sulphate-soot system, *Atmos. Environ.*, *31*, 1393–1402, 1997.

Feichter, J., U. Lohmann, and I. Schult, The atmospheric sulfur cycle in ECHAM-4 and its impact on the short-wave radiation, *Clim. Dyn.*, *13*, 235–246, 1997.

Fiedler, F., I. Bischoff-Gauß, N. Kalthoff, and G. Adrian, Modeling of transport and diffusion of a tracer in the Freiburg-Schauinsland area, *J. Geophys. Res.*, *105*, 1599–1610, 2000.

Fuller, K., W. Malm, and S. Kreidenweis, Effects of mixing on extinction by carbonaceous particles, *J. Geophys. Res.*, *104*, 15,941–15,954, 1999.

Graßl, H., Radiative effects of atmospheric aerosol particles, in *Aerosol and Climate*, edited by P. Hobbs and M. McCormick, pp. 241–252, A. Deepak, Hampton, Va., 1988.

Hale, G., and M. Querry, Optical constants of water in the 200-nm to 200-μm wavelength region, *Appl. Opt.*, *12*, 555–563, 1973.

Hamilton, R., and T. Mansfield, Airborne particulate elemental carbon: Its sources, transport and contribution to dark smoke and soiling, *Atmos. Environ.*, *25*, 715–723, 1991.

Hammer, M.-U., Photochemische Indikatoren zur Charakterisierung der Oxidantienbildung bei Hochdruckwetterlagen, Ph.D. thesis, Inst. für Meteorol. und Klimaforsch. der Univ. Karlsruhe (TH), Karlsruhe, Germany, 2001.

Hänel, G., The properties of atmospheric aerosol particles as functions of the relative humidity at thermodydamic equilibrium with the surrounding moist air, *Adv. Geophys.*, *19*, 74–188, 1976.

Hess, M., P. Koepke, and I. Schult, Optical properties of aerosols and clouds: The software package OPAC, *Bull. Am. Meteorol. Soc.*, *79*, 831–844, 1998.

Hitzenberger, R., and S. Tohno, Comparison if black carbon (BC) aerosols in two urban areas: Concentrations and size distributions, *Atmos. Environ.*, *35*, 2153–2167, 2001.

Horvath, H., Atmospheric light absorption: A review, *Atmos. Environ., Part A*, *27*, 293–317, 1993.

Horvath, H., Spectral extinction coefficients of rural aerosol in southern Italy: A case study of cause and effect of variability of atmospheric aerosol, *J. Aerosol Sci.*, *27*, 437–453, 1996.

Hughes, L., J. Allen, P. Bhave, M. Kleeman, G. Cass, D.-Y. Liu, D. Fergenson, B. Morrical, and K. Prather, Evolution of atmospheric particles along trajectories crossing the Los Angeles Basin, *Environ. Sci. Technol.*, *34*, 3058–3068, 2000.

Intergovernmental Panel on Climate Change (IPCC), *Climate Change 2001: The Scientific Basis*, edited by J. T. Houghton et al., Cambridge Univ. Press, New York, 2001.

Jacobson, M., Development and application of a new air pollution modeling system: II. Aerosol module structure and design, *Atmos. Environ.*, *31*, 131–144, 1997a.

Jacobson, M., Development and application of a new air pollution modeling system: III. Aerosol-phase simulations, *Atmos. Environ.*, *31*, 587–608, 1997b.

Jacobson, M., Studying the effect of aerosols on vertical photolysis rate coefficient and temperature profiles over an urban airshed, *J. Geophys. Res.*, *103*, 10,593–10,604, 1998.

Jacobson, M., A physically based treatment of elemental carbon optics: Implications for global direct forcing of aerosols, *Geophys. Res. Lett.*, *27*, 217–220, 2000.

Jacobson, M., Strong radiative heating due to the mixing state of black carbon in atmospheric aerosols, *Nature*, *409*, 695–697, 2001.

Jacobson, M. Z., Control of fossil-fuel particulate black carbon and organic matter, possibly the most effective method of slowing global warming, *J. Geophys. Res.*, *107*(D19), 4410, doi:10.1029/2001JD001376, 2002.

Jacobson, M., R. Turco, E. Jensen, and O. Toon, Modeling coagulation among particles of different composition and size, *Atmos. Environ.*, *28*, 1327–1338, 1994.

Kamm, S., O. Möhler, K.-H. Naumann, H. Saathoff, and U. Schurath, Heterogenous interaction of ozone, NO_2 and N_2O_5 with soot aerosol, *Atmos. Environ.*, *33*, 4651–4661, 1999.

Kleeman, M., G. Cass, and A. Eldering, Modeling the airborne particle complex as a source-oriented external mixture, *J. Geophys. Res.*, *102*, 21,355–21,372, 1997.

Kotzick, R., and R. Nießner, The effect of aging processes on critical supersaturation ratios of ultrafine carbon aerosols, *Atmos. Environ.*, *33*, 2669–2677, 1999.

Lamb, B., A. Guenther, D. Gay, and H. Westberg, A national inventory of biogenic hydrocarbon emissions, *Atmos. Environ.*, *21*, 1695–1705, 1987.

Lesins, G., P. Chylek, and U. Lohmann, A study of internal and external mixing scenarios and its effect on aerosol optic properties and direct radiative forcing, *J. Geophys. Res.*, *107*(D10), 4094, doi:10.1029/2001JD000973, 2002.

Liepert, B., and I. Tegen, Multidecadal solar radiation trends in the United States and Germany and direct tropospheric aerosol forcing, *J. Geophys. Res.*, *107*(D12), 4153, doi:10.1029/2001JD000760, 2002.

Liousse, C., J. Penner, C. Chuang, J. Walton, H. Eddleman, and H. Cachier, A global three-dimensional model study of carbonaceous aerosols, *J. Geophys. Res.*, *101*, 19,411–19,432, 1996.

Ludwig, J., F. X. Meixner, B. Vogel, and J. Förstner, Soil-air exchange of nitric oxide: An overview of processes, environmental factors, and modeling studies, *Biogeochemistry*, *52*, 225–258, 2001.

Markowicz, K. M., P. J. Flatau, M. V. Ramana, P. J. Crutzen, and V. Ramanathan, Absorbing Mediterranean aerosols lead to a large reduction in the solar radiation at the surface, *Geophys. Res. Lett.*, *29*(20), 1968, doi:10.1029/2002GL015767, 2002.

McKeen, S., E.-Y. Hsie, and S. C. Liu, A study of the dependence of rural ozone on ozone precursors in the eastern United States, *J. Geophys. Res.*, *96*, 15,377–15,394, 1991.

Mehlmann, A., and P. Warneck, Atmospheric gaseous HNO_3, particulate nitrate, and aerosol size distributions of major ionic species at a rural site in western Germany, *Atmos. Environ.*, *29*, 2359–2373, 1995.

Mészáros, E., T. Barcza, A. Gelencsér, J. Hlavay, G. Kiss, Z. Krivácsy, A. Molnár, and K. Polyák, Size distributions of inorganic and organic species in the atmospheric aerosol in Hungary, *J. Aerosol Sci.*, *28*, 1163–1175, 1997.

Nakajima, T., and M. Tanaka, Matrix formulations for the transfer of solar radiation in a plan-parallel scattering atmosphere, *J. Quant. Spectrosc. Radiat. Transfer*, *35*, 13–21, 1986.

Naoe, H., and K. Okada, Mixing properties of submicrometer aerosol particles in the urban atmosphere: With regard to soot particles, *Atmos. Environ.*, *35*, 5765–5772, 2001.

Nester, K., H.-J. Panitz, and F. Fiedler, Comparison of the DRAIS and EURAD model simulations of air pollution in a mesoscale area, *Meteorol. Atmos. Phys.*, *57*, 135–158, 1995.

Neusüß, C., H. Wex, W. Birmili, A. Wiedensohler, C. Koziar, B. Busch, E. Brüggemann, T. Gnauk, M. Ebert, and D. S. Covert, Characterization and parameterization of atmospheric particle number-, mass-, and chemical-size distributions in central Europe during LACE 98 and MINT, *J. Geophys. Res.*, *107*(D21), 8127, doi:10.1029/2001JD000514, 2002.

Obermeier, A., R. Friedrich, C. John, J. Seier, H. Vogel, F. Fiedler, and B. Vogel, *Photosmog: Möglichkeiten und Strategien zur Verminderung des bodennahen Ozons, Umweltforschung in Baden-Württemberg*, Ecomed, Landsberg, Germany, 1995.

Okada, K., and R. Hitzenberger, Mixing properties of individual submicrometer aerosol particles in Vienna, *Atmos. Environ.*, *35*, 5617–5628, 2001.

Penner, J., H. Eddleman, and T. Novakov, Towards the development of a global inventory for black carbon emissions, *Atmos. Environ.*, *27*, 1277–1295, 1993.

Possanzini, M., F. D. Santis, and V. D. Palo, Measurements of nitric acid and ammonium salts in lower Bavaria, *Atmos. Environ.*, *33*, 3597–3602, 1999.

Pregger, T., et al., Entwicklung von Instrumenten zur Analyse der Umweltbelastungen durch Feinstäube und andere ausgewählte Luftverunreinigungen in Baden-Württemberg, *FZKA-BWPLUS-50*, Baden-Württemberg Programm Lebensgrundlage Umwelt und ihre Sicherung (BWPLUS), Forschungszent. Karlsruhe, Karlsruhe, Germany, 1999.

Ramanathan, V., et al., Indian Ocean Experiment: An integrated analysis of the climate forcing and effects of the great Indo-Asian haze, *J. Geophys. Res.*, *106*, 28,371–28,398, 2001.

Reuder, J., T. Gori, L. Kins, and R. Dlugi, Determination of photolysis frequencies of ozone and nitrogen dioxide during SANA: 2. The influence of tropospheric aerosol particles, *Meteorol. Z. N. F.*, *5*, 234–244, 1996.

Riemer, N., Numerische Simulationen zur Wirkung des Aerosols auf die Troposphärische Chemie und die Sichtweite, Ph.D. thesis, Inst. für Meteorol. und Klimaforsch. der Univ. Karlsruhe (TH), Karlsruhe, Germany, 2002.

Ruggaber, A., R. Dlugi, and T. Nakajiima, Modelling radiation quantities and photolysis frequencies in the troposphere, *J. Atmos. Chem.*, *18*, 171–210, 1994.

Russell, P., et al., Overview of ACE-Asia spring 2001 investigations on aerosol-radiation interactions, paper presented at Joint CACGP/IGAC 2002 International Symposium, Comm. on Atmos. Chem. and Global Pollut., Crete, Greece, 2002.

Schaap, M., K. Müller, and H. ten Brink, Constructing the European aerosol nitrate concentration field from quality analysed data, *Atmos. Environ.*, *36*, 1323–1335, 2002.

Schädler, G., Triggering of atmospheric circulations by moisture inhomogeneities of the Earth's surface, *Boundary Layer Meteorol.*, *51*, 1–29, 1989.

Schell, B., I. Ackermann, F. Binkowski, and A. Ebel, Modeling the formation of secondary organic aerosol within a comprehensive air quality model system, *J. Geophys. Res.*, *106*, 28,275–28,293, 2001.

Schnaiter, M., H. Horvath, O. Möhler, K.-H. Naumann, H. Saathoff, and O. Schöck, UV-VIS-NIR spectral optical properties of soot and soot-containing aerosols, *J. Aerosol Sci.*, in press, 2003.

Seier, J., P. Berner, R. Friedrich, C. John, and A. Obermeier, Generation of an emission data base for TRACT, in *Exchange and Transport of Air Pollutants Over Complex Terrain and the Sea*, edited by S. Larsen, F. Fiedler, and P. Borell, pp. 269–278, Springer-Verlag, New York, 2000.

Seland, O., and R. Iversen, A scheme for black carbon and sulphate aerosols tested in a hemispheric scale, Eulerian dispersion model, *Atmos. Environ.*, *33*, 2853–2879, 1999.

Sloane, C., Optical properties of aerosols of mixed composition, *Atmos. Environ.*, *18*, 871–878, 1984.

Stockwell, W., P. Middleton, and J. S. Chang, The second generation regional acid deposition model chemical mechanism for regional air quality modeling, *J. Geophys. Res.*, *95*, 16,343–16,367, 1990.

Stroem, J., K. Okada, and J. Heintzenberg, On the state of mixing of particles due to Brownian coagulation, *J. Aerosol Sci.*, *23*, 467–480, 1992.

Taylor, K., and J. Penner, Response of the climate system to atmospheric aerosols and greenhouse gases, *Nature*, *369*, 734–737, 1994.

Toon, O., and J. Pollak, The optical constants of several atmospheric aerosol species: Ammonium sulfate, aluminium oxide, and sodium chloride, *J. Geophys. Res.*, *81*, 5733–5748, 1976.

Van Dingenen, R., J.-P. Putaud, A. Dell'Acqua, S. M.-D. Santos, J. Viidanoja, and F. Raes, Physical and chemical aerosol properties at an urban and a rural site during an episode of strong photochemical activity during ESCOMPTE, paper presented at XXVII General Assembly, Eur. Geophys. Soc., Nice, France, 21–26 April, 2002.

Vogel, B., F. Fiedler, and H. Vogel, Influence of topography and biogenic volatile organic compounds emission in the state of Baden-Württemberg on ozone concentrations during episodes of high air temperatures, *J. Geophys. Res.*, *100*, 22,907–22,928, 1995.

Vogt, R., V. Scheer, and C. Rehbein, Measurement of exhaust particles: A comparison of the emission lab and atmosphere, paper presented at IAA Technical Congress, Int. Automobilausstellung, Frankfurt, Germany, 2000.

Weingartner, E., H. Burtscher, and H. Baltensperger, Hygroscopic properties of carbon and diesel soot particles, *Atmos. Environ.*, *31*, 2311–2327, 1997.

Wendisch, M., J. Heitzenberg, and M. Bussmer, Measurement-based aerosol forcing calculations: The influence of model complexity, *Meteorol. Z. N. F.*, *10*, 45–60, 2001.

Wex, H., C. Neusüß, M. Wendisch, F. Stratmann, C. Koziar, A. Keil, A. Wiedensohler, and M. Ebert, Particle scattering, backscattering, and absorption coefficients: An in situ closure and sensitivity study, *J. Geophys. Res.*, *107*(D21), 8122, doi:10.1029/2000JD000234, 2002.

Whitby, E., P. McMurray, U. Shankar, and F. Binkowski, Modal aerosol dynamics modeling, *Tech. Rep. 600/3-91/020*, Atmos. Res. and Exposure Assess. Lab., U.S. Environ. Prot. Agency, Research Triangle Park, N. C., 1991. (Available as *PB91-161729/AS* from Natl. Tech. Inf. Serv., Springfield, Va.)

Wickert, B., U. Schwarz, P. Blank, C. John, J. Kühlwein, A. Obermeier, and R. Friedrich, Generation of an emission data base for Europe 1994, in *Proceedings of EUROTRAC Symposium'98*, edited by P. M. Borrell and P. Borrell, vol. 2, pp. 255–260, WIT Press, Boston, Mass., 1999.

Wilson, J., C. Cuvelier, and F. Raes, A modeling study of global mixed aerosol fields, *J. Geophys. Res.*, *106*, 34,081–34,108, 2001.

Yienger, J., and H. Levy, Empirical model of global soil-biogenic NO_x emissions, *J. Geophys. Res.*, *100*, 11,447–11,464, 1995.

Zappoli, S., et al., Inorganic, organic and macromolecular components of fine aerosol in different areas of Europe in relation to their water solubility, *Atmos. Environ.*, *33*, 2733–2743, 1999.

Zhang, Y., C. Seigneur, J. Seinfeld, M. Jacobson, and F. Binkowski, Simulation of aerosol dynamics: A comparative review of algorithms used in air quality models, *Aerosol Sci. Technol.*, *31*, 487–514, 1999.

F. Fiedler, B. Vogel, and H. Vogel, Institut für Meteorologie und Klimaforschung, Forschungszentrum Karlsruhe, P. O. Box 3640, 76021 Karlsruhe, Germany. (franz.fiedler@imk.fzk.de; bernhard.vogel@imk.fzk.de; heike.vogel@imk.fzk.de)

N. Riemer, Department of Mechanical and Aeronautical Engineering, University of California, Davis, One Shields Avenue, Davis, CA 95616-5294, USA. (nsriemer@ucdavis.edu)